Mon. Not. R. Astron. Soc. **000**, 1–?? () Printed 29 January 2015 (MN LATEX style file v2.2)

Phase space dynamics of triaxial collapse: II. Universal evolution of axis ratios

Sharvari Nadkarni-Ghosh[1⋆] and Akshat Singhal[2]†
[1] *Department of Physics, I.I.T. Kanpur, Kanpur, U.P. 208016 India*
[2] *Department of Mathematics and Statistics, I.I.T. Kanpur, Kanpur, U.P. 208016 India*

ABSTRACT
In paper I of this series, we examined triaxial collapse in terms of the dynamics of eigenvalues of three important tensors: the Hessian of the gravitational potential, the tensor of velocity derivatives and the deformation tensor. The first paper focussed on the joint gravity-velocity dynamics and here we focus on the deformation tensor, which is directly related to the axes' evolution. We examine the evolution of the minor to major and intermediate to major axes ratios (s and q) and the triaxiality parameter T as function of mass scale and redshift. We find that the ellipticity and prolateness increase with decreasing mass scale and decreasing redshift. These trends, while in agreement with previous analytic studies, contradict numerical simulations. Nevertheless, we find that a suitable transformation of s, motivated by the scaling used in recent analysis of the Millennium XXL simulations by Bonamigo *et al* (2014), has a universal log-normal distribution function that matches their numerical results. Similarly, the transformation $\tilde{q} = (q-s)/(1-s)$ also has a universal beta distribution that is valid over a decade in mass range and over a wide range of redshift scales, indicating that the variable $\tilde{q}$ can be thought of as an invariant of the phase space dynamics.

Key words: cosmology: large-scale structure of Universe

1 INTRODUCTION

Observations have established beyond any doubt that dark matter haloes are well described by a triaxial geometry. The evidence has come from a variety of probes including the optical and X-ray surface brightness, indirect observations though the Sunyaev-Zeldovich effect and weak and strong gravitational lensing (see review by Limousin et al. 2013 and references therein). Numerical simulations have also confirmed triaxiality (e.g., Jing & Suto 2002; Allgood et al. 2006; Schneider et al. 2012) and ellipsoidal halo-shape finders have proven to give more realistic haloes than their spherical counterparts (Despali, Tormen, & Sheth 2013). The motivation for understanding the shape, structure and dynamics of haloes is two-fold. In the currently accepted hierarchical model of structure formation small scale structures collapse first and larger structures are formed through mass accretion and major mergers. The details of the halo shape distribution provide useful information regarding this process of structure formation and evolution. The second major reason is from the point of view of precision cosmology. For example, understanding the systematics due to intrinsic ellipticity correlations is a crucial part of any weak lensing measurement (e.g., Refregier 2003; Oguri & Keeton 2004; Joachimi et al. 2013) and important in determining the Hubble constant from cluster shapes (Wang & Fan 2006; Kawahara et al. 2008). Cluster and void ellipticities have also been proposed as a probe to constrain cosmological parameters such as σ_8 and the dark energy equation of state (Ho et al. 2006; Lee 2006; Park & Lee 2007; Lavaux & Wandelt 2010).

Over the years, numerical simulations have become increasingly sophisticated and efficient at the task of modeling dark matter halo shapes (Dubinski & Carlberg 1991; Bullock 2002; Jing & Suto 2002; Kasun & Evrard 2005; Hopkins, Bahcall, & Bode 2005; Allgood et al. 2006; Schneider, Frenk, & Cole 2012; Despali, Giocoli, & Tormen 2014; Bonamigo et al. 2014).

⋆ E-mail: sharvari@iitk.ac.in
† E-mail: akshat.singhal014@gmail.com

Using this information for precision cosmology involves exploring a large range of parameter space and the computational cost involved in N-body codes proves to be a significant drawback. Furthermore, as was pointed out by Allgood et al. (2006), various groups differ in their methodology of determining halo shapes and hence differ in their results. Thus, the need for analytic investigations still remains.

Triaxial collapse in an expanding universe has been under study for over four decades (Icke 1973; White & Silk 1979; Nariai & Fujimoto 1972; Eisenstein & Loeb 1995; Bond & Myers 1996; Lithwick & Dalal 2011). Various authors have considered it specifically in the context of axis ratio evolution. The seminal paper by Bardeen et al. (1986) used excursion set theory to compute the ellipticity and prolateness distribution of dark matter haloes forming under gravitational collapse of initial Gaussian random fields. Lee, Jing, & Suto (2005) combined the dynamics given by the Zeldovich approximation with the statistical properties of the linear field to obtain the probability distributions of axis ratios. Sandvik et al. (2007) and Desjacques (2008) have used excursion sets to model the effect of the environment on halo ellipticity.

Recent work by the authors (Nadkarni-Ghosh & Singhal 2014, hereafter paper I) analysed triaxial collapse in terms of the coupled dynamics of eigenvalues of three tensors: the Hessian of the gravitational potential, the tensor of derivatives of the velocity field and the deformation tensor. Paper I focussed on the joint dynamics of the gravitational and velocity fields. This paper focuses on the dynamics of the deformation tensor, which gives direct information about the evolution of the axis ratios. We start by reviewing the phase space equations and establish the notation (§2). The details of the numerical runs are described next (§3). The shape of the triaxial object is quantified using three parameters: the minor to major axis ratio, s, the intermediate to major axis ratio, q, and the triaxiality parameter (Franx, Illingworth, & de Zeeuw 1991), T. These are defined in terms of the eigenvalues of the deformation tensor; the dynamics of the latter is completely determined by the phase space equations. §4 gives the results and we discuss and conclude in §5

2 THE PHASE SPACE EQUATIONS

The physical system consists of a homogenous isolated ellipse evolving in a cosmological background consisting only of dark matter and dark energy with an equation of state $w = -1$ (ΛCDM). In the absence of rotations, the evolution of the ellipse is completely determined by the three tensors: the Hessian of the gravitational potential, the tensor of velocity derivatives and the deformation tensor. Let $\lambda_{d,i}, \lambda_{v,i}$ and $\lambda_{a,i}$ {i=1,2,3}, denote the eigenvalues of these three tensors respectively. The dynamics of these nine variables is given by (see paper I for details)

$$\frac{d\lambda_{a,i}}{d\ln a} = -\lambda_{v,i}(1-\lambda_{a,i}) \tag{1a}$$

$$\frac{d\lambda_{v,i}}{d\ln a} = -\frac{1}{2}\left[3\Omega_m(a)\lambda_{d,i} - \{\Omega_m(a) - 2\Omega_\Lambda(a) - 2\}\,\lambda_{v,i} + 2\lambda_{v,i}^2\right] \tag{1b}$$

$$\begin{aligned}\frac{d\lambda_{d,i}}{d\ln a} = &-(1+\delta)\left(\delta+\frac{5}{2}\right)^{-1}\left(\lambda_{d,i}+\frac{5}{6}\right)\sum_{j=1}^{3}\lambda_{v,j} \\ &+\left(\lambda_{d,i}+\frac{5}{6}\right)\sum_{i=1}^{3}(1+\lambda_{v,i}) - \left(\delta+\frac{5}{2}\right)(1+\lambda_{v,i}) \\ &+\sum_{j\neq i}\frac{\{\lambda_{d,j}-\lambda_{d,i}\}\cdot\left\{(1-\lambda_{a,i})^2(1+\lambda_{v,i}) - (1-\lambda_{a,j})^2(1+\lambda_{v,j})\right\}}{(1-\lambda_{a,i})^2-(1-\lambda_{a,j})^2},\end{aligned} \tag{1c}$$

where

$$\delta = \sum_{i=1}^{3}\lambda_{d,i}.$$

Let a be the scale factor of the background and a_i be the scale factors corresponding to the three axes of the ellipsoid. The three λ_is and a_is are related as

$$\lambda_{a,i} = 1 - \frac{a_i}{a} \tag{2a}$$

$$\lambda_{v,i} = \frac{1}{H}\frac{\dot{a}_i}{a_i} - 1 \tag{2b}$$

$$\lambda_{d,i} = \frac{\delta\alpha_i}{2} + \lambda_{ext,i}, \tag{2c}$$

where

$$\alpha_i = a_1a_2a_3\int_0^\infty \frac{d\tau}{(a_i^2+\tau)\prod_{j=1}^{j=3}(a_j^2+\tau)^{1/2}} \quad \text{with} \quad \left(\sum_{i=1}^{3}\alpha_i = 2\right) \tag{3}$$

$$\lambda_{ext,i} = \frac{5}{4}\left(\alpha_i - \frac{2}{3}\right) \quad \text{non-linear approx.} \tag{4}$$

σ_G	$R_{f,Gauss}(h^{-1}\mathrm{Mpc})$	$M_{f,Gauss}(10^{14}M_\odot)$
0.5	14.26	5.30
0.6	12.04	3.18
0.8	9.05	1.34
0.9	8	0.91
1	7.12	0.65
1.2	5.77	0.34

Table 1. Relation between the r.m.s. σ_G and the mass scale M_f for a BBKS power spectrum with spectral index $n_s = 1$ (Dodelson 2003) and a Gaussian filter $W(kR_f) = e^{-\frac{k^2R_f^2}{2}}$. The power spectrum was normalized such that $\sigma_8 = 0.9$.

and the evolution of Ωs is given by

$$\Omega_m(a) = \frac{\Omega_{m,0}H_0^2a_0^3}{H^2a^3}; \quad \Omega_\Lambda(a) = 1 - \Omega_m(a) \tag{5}$$

The subscripts '0' denotes the value today. At early times, when the fluctuations are small, $\lambda_{d,i} = \lambda_{a,i}$ and $\lambda_{v,i} = -f(\Omega_m)\lambda_{d,i}$, where $f(\Omega_m)$ is the linear growth rate, usually approximated as $f(\Omega_m) \approx \Omega_m^{0.55}$ for a ΛCDM cosmology (Linder 2005). The equations above were derived from the triaxial dynamics model of Bond & Myers (1996).

3 NUMERICAL RUNS

For Gaussian initial conditions, the initial distribution of the $\lambda_{d,i}$ is given by Doroshkevich (1970)

$$p(\lambda_{d,1},\lambda_{d,2},\lambda_{d,3}) = \frac{15^3}{8\pi\sqrt{5}\sigma_G^6}\exp\left(-\frac{3I_1^2}{\sigma_G^2} + \frac{15I_2}{2\sigma_G^2}\right) \times (\lambda_{d,1}-\lambda_{d,2})(\lambda_{d,2}-\lambda_{d,3})(\lambda_{d,1}-\lambda_{d,3}) \tag{6}$$

where σ_G is the r.m.s. fluctuation at the scale R_f, $I_1 = \lambda_{d,1} + \lambda_{d,2} + \lambda_{d,3}$ and $I_2 = \lambda_{d,1}\lambda_{d,2} + \lambda_{d,2}\lambda_{d,3} + \lambda_{d,1}\lambda_{d,3}$. This distribution only assumes Gaussianity and does not depend on the details of the power spectrum. The power spectrum is relevant when relating σ_G to a mass or radius scale:

$$\sigma_G^2(R_f,z) = \frac{1}{(2\pi)^3}\int P(k,z)W^2(kR_f)d^3k, \tag{7}$$

where $P(k,z)$ is the linear power spectrum at redshift z and depends on the power spectrum at redshift zero through the linear growth factor (Dodelson 2003) and $W(kR_f)$ is the window function. The mass scale M_f is related to smoothing scale R_f as $M_f = 4\pi/3R_f^3\bar{\rho}_m$, where $\bar{\rho}_m$ is the homogenous background matter density. Table 1 gives the relation between σ_G, radius and mass scales for the BBKS power spectrum (Bardeen et al. 1986) with a Gaussian window function. We considered five different values of $\sigma_G : 0.5, 0.6, 0.8, 1$ and 1.2, which covers a decade in mass scales. For each value of σ_G five realizations were drawn, each consisting of 10^4 points. We focussed only on those initial points which correspond to overdense regions and are mildly non-linear today ($a_0 = 1$). This roughly corresponds to initial δ values which lie within one standard deviation. At the initial time, chosen to be $a_{init} = 0.001$, the system is linear and $\Omega_m \approx 1$, implying $\lambda_{a,i}(a_{init}) = \lambda_{d,i}(a_{init})$, $\lambda_{v,i}(a_{init}) = -\lambda_{d,i}(a_{init})$. The initial conditions were evolved from $a = a_{init}$ to $a = 1$ using the system of eqs. (1). The shape parameters of the ellipse at any intermediate time can be constructed from the λ_as.

The shape of a triaxial object is completely characterized by two parameters (a third parameter will correspond to setting the scale of the object). It is customary to use the ratios of smallest to largest and intermediate to largest axes defined as

$$s = \frac{a_{min}}{a_{max}} \tag{8}$$

$$q = \frac{a_{inter}}{a_{max}}, \tag{9}$$

where a_{min}, a_{max} and a_{inter} are the smallest, largest and intermediate axis respectively. In terms of the λ_a parameters, these are

$$s = \frac{1-\lambda_{a,max}}{1-\lambda_{a,min}} \tag{10}$$

$$q = \frac{1-\lambda_{a,inter}}{1-\lambda_{a,min}}. \tag{11}$$

The triaxiality parameter that characterizes the prolateness is defined as (Franx, Illingworth, & de Zeeuw 1991)

$$T = \frac{a_{max}^2 - a_{inter}^2}{a_{max}^2 - a_{min}^2} = \frac{1-q^2}{1-s^2}. \tag{12}$$

Note that T is not an independent parameter, but derived from q and s. Often, in the literature, triaxiality is characterized in terms of the ellipticity e and prolateness p (Bardeen et al. 1986) and haloes are known to populate a triangular region in

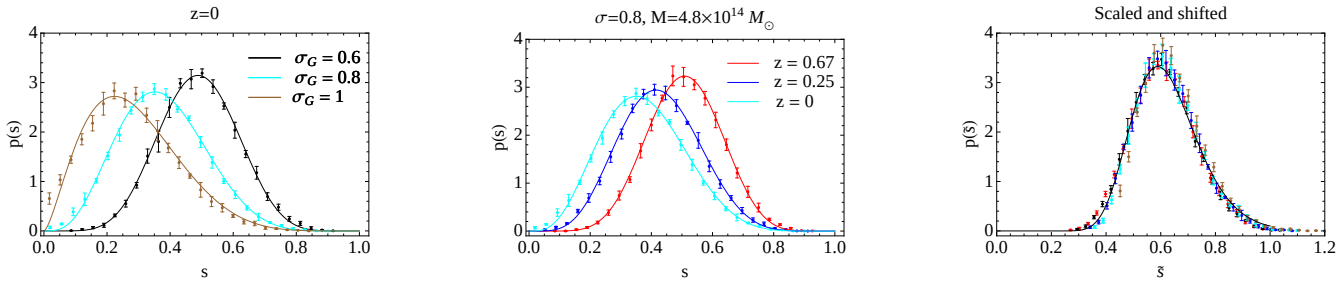

Figure 1. Probability density function of the minor to major axis ratio. The raw PDF is fit by a beta distribution and the scaled and shifted PDF represents has a universal fitting form given by the lognormal distribution.

the $e-p$ space (Porciani, Dekel, & Hoffman 2002; Desjacques 2008; Despali, Giocoli, & Tormen 2014). These are equivalent variables, defined from the eigenvalues of the deformation tensor. While both sets are easy to measure in simulations, s and q have a more direct geometric interpretation. In this paper, we examine the evolution of s, q and T as a function of mass and redshift for a LCDM cosmology. Here we focus only on dark matter overdensities; the investigation of voids is left for future studies. We choose the cosmological parameters in accordance with the ΛCDM cosmology dictated by WMAP-7 (Komatsu et al. 2011): $\Omega_{m,0} = 0.29, \Omega_{\Lambda,0} = 0.71, n_s = 1, \sigma_8 = 0.9, h = 0.73$. The critical density of the universe required to relate the R_f to mass values is $\rho_{c,0} = 2.775h^2 \times 10^{11} M_\odot \mathrm{Mpc}^{-3}$ (Dodelson 2003).

4 RESULTS

Figure 1 shows the probability distribution function (PDF) of s. The left panel shows the variation with mass scale at a given redshift and middle panel shows the variation with redshift for a fixed mass. Smaller mass haloes (larger σ_G) are more elliptical (smaller s) than the larger mass haloes. For a fixed mass scale, the halo ellipticity increases at lower redshifts. This is in agreement with the conclusion reached by Lee et al. (2005) which used the Zeldovich approximation to model the dynamics. Analytic work by Bernardeau (1994) also suggests that rare peaks (more massive objects) are more spherical. However, these conclusions are contrary to the features observed in numerical simulations. This is as expected. Multiple numerical simulations (e.g.,Jing & Suto 2002; Allgood et al. 2006) have shown that accretion and merging play an important role in determining halo ellipticity. Low mass haloes collapse earlier and become more spherical due to accretion and mergers. Therefore, at a given redshift, the lower mass haloes are more spherical than higher mass haloes. Similarly, haloes of similar mass are more elliptical at a higher redshift since mergers are fewer at higher redshifts. The analytic model considered here deals with isolated ellipsoids; the effect of the environment, accretion and merging are not incorporated. Non-linear collapse simply amplifies the initial ellipticity and hence for any halo, ellipticity increases with decreasing redshift.

Although analytical estimates and simulations are in contradiction, we find that a suitable transformation can reconcile the differences. In recent work, Bonamigo et al. 2014 (henceforth B14) analysed the Millennium XXL Simulations (Angulo et al. 2012) and showed that scaling the axis ratio s by an appropriate power of the peak height removed the dependence on mass and redshift resulting in a universal distribution. They considered cluster scale objects $M \sim 10^{14} M_\odot$ which roughly corresponds to the same range of σ_G considered here (see Table 1). Motivated by their results, we examined the effect of such a scaling on the parameter s. We find that pure scaling does not give rise to a universal profile; an additional offset is necessary. Define a new variable [1]

$$\tilde{s} = s\nu^{0.255} + s_0(z, \sigma_G), \tag{13}$$

where the peak height $\nu = \frac{\delta_l}{\sigma_G}$. Here, δ_l is the initial (linear) density of an individual point in the realization and σ_G is the r.m.s. value. The offset parameter $s_0(\sigma_G, z)$ can be interpreted as a model for the physics missing in the analytic picture. Figure 2 shows the offset as a function of z for three different values of σ_G. As expected, the offset is small at high redshifts and for larger mass scales (lower σ_G). This function captures the fact that effect of mergers becomes increasingly important at late times. The scale at which mergers start to dominate also changes with time; lower mass scales are affected at earlier epochs because they collapse first. Fitting the offset as a function of σ_G and z gives

$$s_0(\sigma_G, z) = A(\sigma_G) \log_{10}\left(\frac{1}{1+z}\right) + B(\sigma_G), \tag{14}$$

where $A(\sigma_G) = 0.22\sigma_G + 0.44$ and $B(\sigma_G) = -0.91 \log_{10} \sigma_G + 0.45$. This fit is valid in the range $\sigma_G = 0.5$ to $\sigma_G = 1$ and

[1] We differ in our definition of ν from that of Bonamigo et al. (2014) who use $\nu = \delta_c(z)/\sigma(M)$, where $\delta_c(z)$ is the critical overdensity for collapse and $\sigma(M)$ is the r.m.s. fluctuation on the scale M.

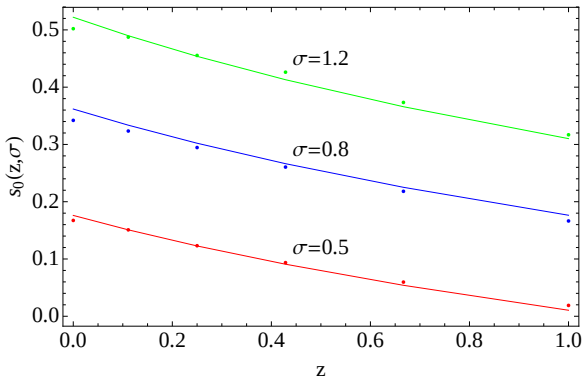

Figure 2. Offset function $s_0(z, \sigma)$. Dots indicate the data points and the solid lines are the fit given by eq. (**??**). This function models the discrepancy between simulations and the analytic model presented here.

the redshift range $z = 1$ to $z = 0$. The PDF of $\tilde{s}$ is shown in the last panel of figure 1. It has a universal form given by the lognormal function.

$$p(\bar{s}, \mu, \sigma) = \frac{1}{x\sqrt{2\pi}\sigma} \exp\{-\frac{(\ln \bar{s} - \mu)^2}{2\sigma^2}\}. \tag{15}$$

with $\mu = -0.49, \sigma = 0.2$, in agreement with that of B14.

Figure 3 shows the PDF of intermediate to major axis ratio. The left and the middle panel show the PDF of the variable q. The definitions of q and s imply that $q > s$ and also $q < 1$. Therefore, for the same mass scale and redshift, q has a narrower distribution than the corresponding s distribution in figure 1. The ratios s and q individually capture the two dimensional eccentricity along a cross-section perpendicular to the intermediate and minor axis respectively. To understand the full 3D geometry, it is generally the conditional probability $p(q|s)$ which is the quantity of interest. Instead of the conditional probability, we consider the PDF of the s-dependent variable defined by Schneider, Frenk, & Cole (2012)

$$\tilde{q} = \frac{q - s}{1 - s}. \tag{16}$$

Their motivation for this transformation was that its range is the unit interval and hence it has the same support as the beta distribution. They considered the conditional probability $p(\tilde{q}|s)$ and found s-dependent but redshift independent beta distributions. We do not consider the conditional probability, i.e., we do not bin in s space, instead we use the s value of the individual density peak (halo) and find that PDF of this transformed variable is independent of mass scale and redshift and also well fit by a beta distribution

$$p(\tilde{q}, \alpha, \beta) = \frac{1}{B(\alpha, \beta)} \tilde{q}^{\alpha-1}(1 - \tilde{q})^{\beta-1}. \tag{17}$$

with parameters $\alpha = 2.52$ an $\beta = 2.56$ over the mass range $\sigma_G = 0.5 - 1.2$ and over the redshift range $z = 99$ to $z = 0$. The agreement at very early times, suggests that this scaling is encoded in the initial distribution, but the universality suggests that the non-linear evolution preserves it. To understand this universality better, we examined the pointwise evolution of $\tilde{q}$ over the entire redshift range from the phase space dynamics. We focus on a single value of σ_G and a single realization. For each point in the realization we examine the difference between the transformed ratio at any epoch $\tilde{q}(a)$ and the ratio today $\tilde{q}_0 = \tilde{q}(a = 1)$. Figure 4 shows the maximum difference over all points in the realization (for $\sigma_G = 0.5$). This gives a conservative estimate of the difference for each epoch. We find that the difference stays small throughout the evolution. Thus, we can conclude that to within about a 1% error, $\tilde{q}$ can be thought of as a invariant of the dynamics. The fact that the difference decreases monotonically is just a consequence of defining the differences with respect to the value today. Whether or not numerical simulations show a similar invariance/universality in the variable $\tilde{q}$ remains to be checked.

Figure 5 shows the distribution of the triaxiality parameter T. A perfectly prolate spheriod is one in which two axes are equal and less than the third ($a_{min} = a_{inter} < a_{max} \implies q = s, T = 1$) and a perfectly oblate spheriod is one where two axes are equal and greater than the third ($a_{min} < a_{inter} = a_{max} \implies q = 1, s < 1, T = 0$). For general triaxial objects with no two axes equal, the range $0 < T < 1/3$ is considered oblate, $2/3 < T < 1$ is considered prolate. Haloes with $1/3 < T < 2/3$ are neither prolate nor oblate (Allgood et al. 2006; Schneider, Frenk, & Cole 2012). The left panel of figure 5 shows that at a given redshift, lower mass haloes (higher σ_G) are more prolate than higher masses and the right panel shows that prolateness is higher for lower redshifts. On the other hand, numerical simulations (Schneider, Frenk, & Cole 2012; Despali, Giocoli, & Tormen 2014) and observations (Paz et al. 2011) suggest that most haloes are prolate, the more massive haloes being more prolate. Prolateness also increases with increasing redshift. These contradicting results again highlight the importance of post collapse processes, accounted for in simulations, in determining halo prolateness.

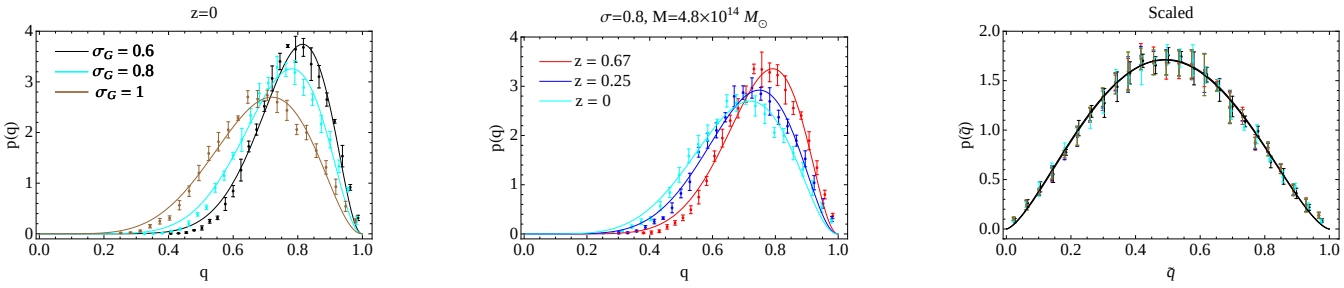

Figure 3. Probability density function of the intermediate to major axis ratio. Both the raw and the scaled PDFs follow the beta distribution. The latter is a universal profile with parameters $\alpha = 2.52$ and $\beta = 2.56$.

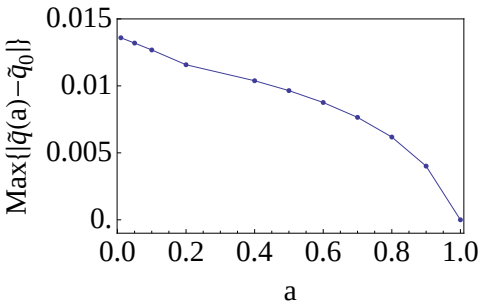

Figure 4. $\tilde{q}$ as an invariant of the dynamics. $\tilde{q}(a) - \tilde{q}_0$ gives a measure of the change in $\tilde{q}$ for each point in the realization. The maximum over all points in the realization gives a conservative estimate of the overall change. The difference stays small throughout the evolution indicating that $\tilde{q}$ may be treated as an invariant of the phase space dynamics.

5 DISCUSSION AND CONCLUSION

We have investigated the evolution of axis ratios using the dynamics of the eigenvalues of the deformation tensor. The eigenvalues are directly related to three parameters which quantify the shape of the triaxial object: the ratio of minor to major axis s, the ratio of intermediate to major axis q, and the triaxiality parameter T, which quantifies prolateness vs. oblateness. We find that, for a given redshift lower mass haloes are more elliptical and more prolate than higher mass haloes and the ellipticity and prolateness decreases with redshift. These trends are opposite to those predicted in simulations, but in agreement with other analytic studies such as Lee et al. (2005). This behavior is expected since it is known that mergers play a very crucial role in determining halo ellipticity. Furthermore, Zhao et al. (2003) have argued that more massive haloes undergo a faster accretion, which may account for partially compensating the trends predicted on the basis of isolated collapse, however, more recent work has suggested a mass independent accretion history (Ludlow et al. 2013).

Inspite of this difference, we find that in transformed variables, we obtain a universal behavior for the two axial ratios. This is the main new result of this work. Motivated by the scaling proposed in B14, we find that the transformed variable

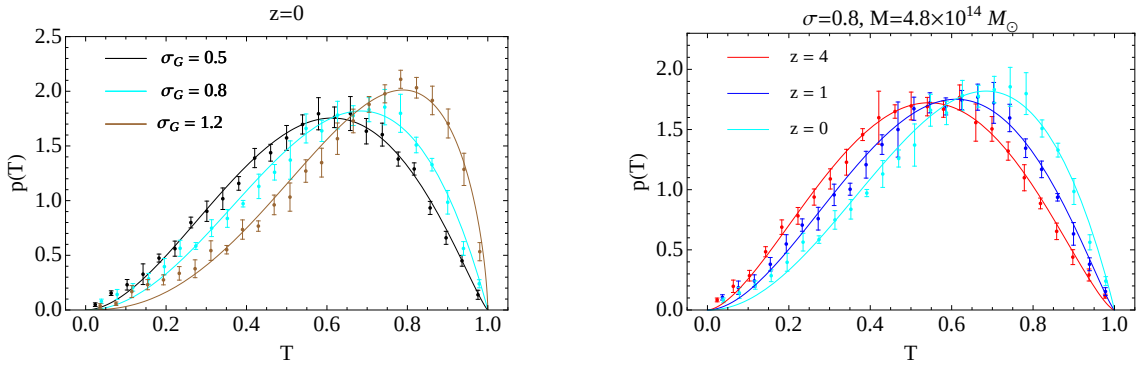

Figure 5. Probability density function of the triaxiality parameter T. The tendency for prolateness increases with decreasing redshift and decreasing mass.

$\tilde{s} = s\nu^{0.255} + s_0(z, \sigma)$, where ν is the peak height, has a universal log-normal profile. The main difference between the scaled variable $\tilde{s}$ of B14 and ours is the additional offset $s_0(z, \sigma)$. This offset function can be thought to capture the missing physics of mergers and accretion and can be used to gain insights while building a more complete analytic model. The second transformed variable $\tilde{q} = (q - s)/(1 - s)$ proposed by Schneider, Frenk, & Cole (2012) was also found to have a universal PDF given by the beta distribution. By examining the point-wise variation of $\tilde{q}$, we find that the variation in $\tilde{q}$ over the entire redshift range is very minimal indicating that $\tilde{q}$ can be thought to be an invariant of the phase space dynamics. Similar phase space invariants have been studied in the context of density-velocity dynamics (Nadkarni-Ghosh 2013; Nadkarni-Ghosh & Singhal 2014). Whether or not simulations suggest similar invariants remains to be checked. If such invariants exist, then they can be exploited to give additional constraints on cosmological parameters as was demonstrated based on spherical dynamics in Nadkarni-Ghosh (2013). This is left for future investigation.

The dynamical evolution equations used in this work were derived from the triaxial collapse model of of Bond & Myers (1996). This model involves many approximations. The ellipsoid is rotationless and isolated and the effect of external tidal forces is modeled in terms of the axes of the ellipsoid. In order to make more realistic predictions, it will be necessary to consider models such as the one proposed by Desjacques (2008) which more accurately takes into account the effect of the environment and/or employ the formalism developed by Nariai & Fujimoto (1972) and Eisenstein & Loeb (1995) which allows for rotations. The main motivation to build increasingly accurate analytic models, inspite of the increasing accuracy of N-body simulations, comes from the point of view of precision cosmology. Given the range of unconstrained cosmological parameters and the increasing size of data sets, computing time becomes a limiting factor. Analytic alternatives are hence necessary and studies like the one presented here pave the way for more sophisticated model building in the future.

REFERENCES

Allgood B., Flores R. A., Primack J. R., Kravtsov A. V., Wechsler R. H., Faltenbacher A., Bullock J. S., 2006, Monthly Notices of the Royal Astronomical Society, 367, 1781
Angulo R. E., Springel V., White S. D. M., Jenkins A., Baugh C. M., Frenk C. S., 2012, Monthly Notices of the Royal Astronomical Society, 426, 2046
Bardeen J. M., Bond J. R., Kaiser N., Szalay A. S., 1986, The Astrophysical Journal, 304, 15
Bernardeau F., 1994, The Astrophysical Journal, 427, 51
Bonamigo M., Despali G., Limousin M., Angulo R., Giocoli C., Soucail G., 2014, ArXiv e-prints, 1410, 15
Bond J. R., Myers S. T., 1996, Astrophysical Journal Supplement Series, 103, 1
Bullock J. S., 2002, Shapes of Dark Matter Halos. World Scientific Publishing Co. Pte. Ltd., 2002., pp. 109–113
Desjacques V., 2008, Monthly Notices of the Royal Astronomical Society, 388, 638
Despali G., Giocoli C., Tormen G., 2014, Monthly Notices of the Royal Astronomical Society, 443, 3208
Despali G., Tormen G., Sheth R. K., 2013, Monthly Notices of the Royal Astronomical Society, 431, 1143
Dodelson S., 2003, Modern Cosmology. Academic Press, Elsevier
Doroshkevich A. G., 1970, Astrophysics, 6, 320
Dubinski J., Carlberg R. G., 1991, The Astrophysical Journal, 378, 496
Eisenstein D. J., Loeb A., 1995, The Astrophysical Journal, 439, 520
Franx M., Illingworth G., de Zeeuw T., 1991, The Astrophysical Journal, 383, 112
Ho S., Bahcall N., Bode P., 2006, The Astrophysical Journal, 647, 8
Hopkins P. F., Bahcall N. A., Bode P., 2005, The Astrophysical Journal, 618, 1
Icke V., 1973, Astronomy and Astrophysics, 27, 1
Jing Y. P., Suto Y., 2002, The Astrophysical Journal, 574, 538
Joachimi B., Semboloni E., Bett P. E., Hartlap J., Hilbert S., Hoekstra H., Schneider P., Schrabback T., 2013, Monthly Notices of the Royal Astronomical Society, 431, 477
Kasun S. F., Evrard A. E., 2005, The Astrophysical Journal, 629, 781
Kawahara H., Kitayama T., Sasaki S., Suto Y., 2008, The Astrophysical Journal, 674, 11
Komatsu E. et al., 2011, The Astrophysical Journal Supplement Series, 192, 18
Lavaux G., Wandelt B. D., 2010, Monthly Notices of the Royal Astronomical Society, 403, 1392
Lee J., 2006, The Astrophysical Journal, 643, 724
Lee J., Jing Y. P., Suto Y., 2005, The Astrophysical Journal, 632, 706
Limousin M., Morandi A., Sereno M., Meneghetti M., Ettori S., Bartelmann M., Verdugo T., 2013, Space Science Reviews, 177, 155
Linder E. V., 2005, Physical Review D, 72, 43529
Lithwick Y., Dalal N., 2011, The Astrophysical Journal, 734, 100
Ludlow A. D. et al., 2013, Monthly Notices of the Royal Astronomical Society, 432, 1103
Nadkarni-Ghosh S., 2013, Monthly Notices of the Royal Astronomical Society, 428, 1166
Nadkarni-Ghosh S., Singhal A., 2014, ArXiv e-prints, 1407, 1945
Nariai H., Fujimoto M., 1972, Progress of Theoretical Physics, 47, 105
Oguri M., Keeton C. R., 2004, The Astrophysical Journal, 610, 663
Park D., Lee J., 2007, Physical Review Letters, 98, 81301
Paz D. J., Sgró M. A., Merchán M., Padilla N., 2011, Monthly Notices of the Royal Astronomical Society, 414, 2029
Porciani C., Dekel A., Hoffman Y., 2002, Monthly Notices of the Royal Astronomical Society, 332, 339
Refregier A., 2003, Annual Review of Astronomy and Astrophysics, 41, 645
Sandvik H. B., Möller O., Lee J., White S. D. M., 2007, Monthly Notices of the Royal Astronomical Society, 377, 234
Schneider M. D., Frenk C. S., Cole S., 2012, Journal of Cosmology and Astro-Particle Physics, 05, 030
Wang Y.-G., Fan Z.-H., 2006, The Astrophysical Journal, 643, 630
White S. D. M., Silk J., 1979, Astrophysical Journal, 231, 1
Zhao D. H., Jing Y. P., Mo H. J., Börner G., 2003, The Astrophysical Journal Letters, 597, L9